Cooperative Exploration of Heterogeneous UAVs in Mountainous Environments by Constructing Steady Communication

Han Jiang, Yanchun Chang, Liying Yang, Xu Liu, and Yuqing He, *Member*, *IEEE*

***Abstract*—Unmanned aerial vehicles (UAVs) must fly at low altitudes to execute certain missions when operating in complex mountainous areas. However, in these environments, UAVs lose their line-of-sight (LOS) communication with the ground station (GS) due to the obstruction of the mountains and are unable to retransmit information such as video, which will lead to mission failure or affect the flight safety of UAVs. To address this difficulty, this study proposes a cooperative planning method for heterogeneous UAVs by ensuring steady communication based on the shortest total mission time. To accomplish this goal, a relay UAV is positioned to enable indirect but constant LOS connectivity between the mission UAV and the GS. Specifically, to alleviate data storage pressure, a terrain lightweight modeling method is employed. In addition, a new LOS judgment model that constructs communication relay LOS links between communication nodes for complex mountain environments is presented. This study considers different types of UAVs; for the fixed-wing UAV, the minimum turning radius constraints are taken into account to plan a flyable trajectory. The problem is formulated as the multi-step optimization model that accounts for communication constraints, obstacle and collision avoidance, and the performance constraints of heterogeneous UAVs to plan the trajectories of the mission UAV and relay UAV in order to maintain LOS links between the mission UAV and the ground station. Finally, the experimental results demonstrate that the proposed method is effective and ensures the completion of cooperative exploration missions for heterogeneous UAVs in complex mountain environments.**

***Index Terms*—motion and path planning, collision avoidance, heterogeneous unmanned aerial vehicles, communication relay, terrain modeling.**

Manuscript received May 18, 2023; Revised August 7, 2023; Accepted September 4, 2023. This paper was recommended for publication by Editor Aniket Bera upon evaluation of the Associate Editor and Reviewers' comments. This work was supported by the National Natural Science Foundation of China under Grants U22B2041, 91948303, and 61991413; in part by the National Natural Science Foundation of China Innovative Research Group Project under Grant 61821005, in part by the Shenyang Municipal Bureau of Science and Technology under Grant RC210477, in part by the Youth Innovation Promotion Association of the Chinese Academy of Sciences under Grant Y2022065. *(Corresponding author: Liying Yang.)*

Han Jiang and Xu Liu are with the State Key Laboratory of Robotics, Shenyang Institute of Automation, Chinese Academy of Sciences, Shenyang 110016, China, with the Institutes for Robotics and Intelligent Manufacturing, Chinese Academy of Sciences, Shenyang 110016, China, and also with the University of Chinese Academy of Sciences, Beijing 100049, China (e-mail: jianghan@sia.cn; liuxu@sia.cn).

Yanchun Chang, Liying Yang and Yuqing He are with the State Key Laboratory of Robotics, Shenyang Institute of Automation, Chinese Academy of Sciences, Shenyang 110016, China, and also with the Institutes for Robotics and Intelligent Manufacturing, Chinese Academy of Sciences, Shenyang 110016, China (e-mail: changyanchun, yangliying, heyuqing @sia.cn).

Digital Object Identifier (DOI): see top of this page.

I. INTRODUCTION

HETEROGENEOUS multiagent systems composed of different types of unmanned platforms have a wide range of applications in search and rescue, military, transportation, and other fields [1]. In particular, different types of unmanned platforms have different levels of problem-solving capabilities and can solve various complex problems through collaborative heterogeneous intelligence [2].

When performing over-the-horizon observation missions in complex mountainous areas, the mission UAV often has to fly in tortuous mountainous terrain, and the obstruction of the mountains interrupts the communication link between the mission UAV and the ground station (GS). An effective solution to this problem is introducing a relay UAV to build a communication relay link between the mission UAV and the GS, as a UAV with high maneuverability can be dynamically deployed in an optimal position to perform auxiliary relay missions [3]-[6]. In previous studies, we used multirotor UAVs for experiments; however, their slow flight velocity did not allow them to reach the mission area quickly, and their poor endurance resulted in unsatisfactory experimental results. Therefore, this study considers two types of heterogeneous UAVs. The mission UAV is a fixed-wing UAV with the following advantages: 1) fast flight velocity and the ability to quickly reach the mission area to perform missions; 2) short total mission time and a low energy consumption required for the relay UAV; and 3) high endurance. The relay UAV is a multirotor UAV with the following advantages: 1) flexible flight and quick adjustment of its own position; 2) ability to maintain a hovering status; and 3) no restriction for minimum turning radius [7], [8].

Obtaining the communication strength between arbitrary points in the air and on the ground is important. Communication strength usually depends on the distance and the line-of-sight (LOS) links between nodes. The LOS links have a major influence on the communication strength within the wireless communication coverage [9], [10]. A LOS probability model is proposed to predict the existence of LOS links [11], [12]. However, the aforementioned studies were conducted in environments where the obstacles had regular shapes and were discretely distributed. Therefore, these methods cannot be applied directly to build a LOS model for mountain environments, which is one of the main focuses of this study.

Using a relay UAV as the communication node is challenging, when the mission UAV has a non-line-of-sight (NLOS) status in a complex mountain environment, it is difficult for the relay UAV to maintain the relay function at a fixed posi-

tion for the duration of the process [13], [14]. Therefore, it is necessary to plan the flight trajectory of the relay UAV. To ensure that the relay UAV can maintain its relay function in complex environments, [15], [16] planned the trajectory of the relay UAV such that it facilitated communication between mobile ground nodes and the GS. The aforementioned studies focused on planning the trajectory of the relay UAV, but neglected the planning for the mobile ground nodes. Simultaneous planning of the relay and mission UAV trajectories allows for improved communication results. However, the trajectory planning of heterogeneous UAVs requires the performance constraints of different types of UAVs to be accounted for. For example, fixed-wing UAV has a minimum turning radius constraint, and a multirotor UAV has a velocity constraint [17]-[20]. Therefore, cooperative trajectory planning for multiple heterogeneous UAVs is also a focus of this study.

To manage the complexity of mountainous environments, we performed lightweight modeling of complex mountainous terrain and established a new model to evaluate the existence of LOS links. To implement cooperative planning for heterogeneous UAVs, a new optimization model was developed to plan the trajectories of the mission and relay UAV. When conducting emergency missions in complex mountainous areas, time is usually an urgent matter. To complete this type of mission quickly, this study proposes cooperative planning of heterogeneous UAVs by constructing steady communication links for the purpose of completing mission in the shortest time. First, we build the terrain lightweight model and use a proposed strategy for reducing the error to avoid UAVs colliding with the mountains [21]. Second, an LOS judgment model is built to construct LOS communication relay links between nodes. An LOS link is established when there are no obstacles between communication nodes; thus, LOS communication maximizes the signal strength [22], [23]. Third, we discuss the constraints based on minimum turning radius trajectory smoothing [24]. Finally, we establish an optimization model that accounts for LOS constraints, obstacle and collision avoidance, heterogeneous UAVs performance constraints, and the mission reference path, which is planned using the A-Star algorithm [25]. We address the optimization problem with the particle swarm optimization algorithm to plan the trajectory [26]. The primary contributions of this study are summarized as follows.

1) We propose a strategy for reducing the error causing by the terrain lightweight model, which avoiding UAVs colliding with the mountain during actual flight.
2) We propose a new model to judge the existence of LOS links to handle the complexity of building the channel model in unstructured mountainous environments.
3) We account for the minimum turning radius constraints to ensure that the fixed-wing UAV has a flyable trajectory, analyze extreme situations in which the trajectory smoothing method based on the minimum turning radius fails, and provide the corresponding treatment measures.
4) We propose a cooperative planning strategy for heterogeneous UAVs in which the mission UAV adjusts its position to cooperate with the relay UAV. The mission efficiency is improved via a new optimization model that autonomously and simultaneously plans the trajectories of the mission UAV and relay UAV.

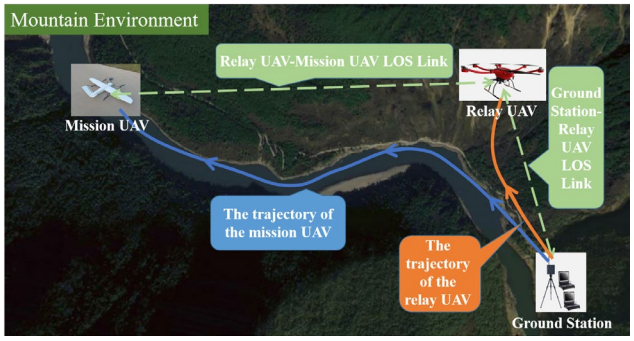

Fig. 1. Mission scenario considered in this study.

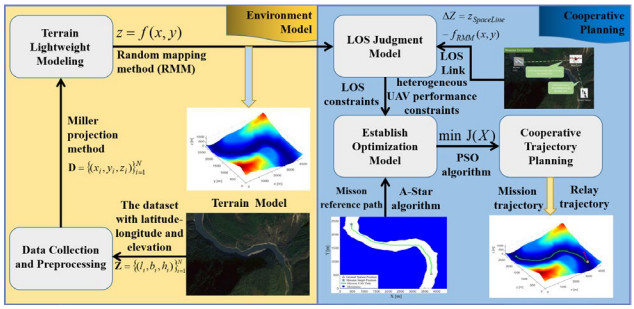

Fig. 2. Overview of cooperative trajectory planning in the mountainous environment considered in this study.

The remainder of this paper is organized as follows. Section II describes the mission scenario and provides an overview of the cooperative trajectory planning approach. Section III explains the terrain modeling method, which uses the random mapping method. Section IV establishes the LOS judgment model, and the minimum turning radius constraints are presented in Section V. Section VI introduces the cooperative trajectory planning. Section VII discuss the experimental results, and Section VIII presents conclusions and future work.

II. Problem Overview

A. Scenarios

The mission scenario considered in this study is illustrated in Fig. 1. In this scenario, there is a mission UAV, a relay UAV, and a stationary ground station (GS), and the mountain environment is known. The mission UAV flies at a low altitude along the river, and the relay UAV flies along a trajectory that allows it to maintain wireless communication between the mission UAV and GS.

B. Overview of Cooperative Trajectory Planning

Fig. 2 shows an overview of the cooperative trajectory planning of heterogeneous multi-UAVs in the mountainous environment considered in this study. First, we extracted the latitude-longitude and elevation information from Google Earth offline map. Subsequently, the Miller projection method was used to obtain a dataset in the local coordinate system [27]. For the dataset, the random mapping method (RMM) was applied to project the irregular points in the low-dimensional dataset into a high-dimensional one to obtain a high-dimensional linear model of the terrain. To create LOS links between nodes, an LOS judgment model was established by combining space-line equations with a high-dimensional linear terrain model. Using this LOS judgment model, the

performance constraints of the heterogeneous UAVs, and the mission reference path that was planned using the A-Star algorithm, an optimization model was established based on the shortest total mission time. Finally, the optimization problem was solved using a particle swarm optimization algorithm to plan the trajectories of the mission UAV and relay UAV.

III. Terrain Lightweight Modeling

A. Terrain Modeling Using the Random Mapping Method

After the data was collected and preprocessed, we acquired the dataset $\mathbf{D} = \{(x_i, y_i, z_i)\}_{i=1}^{N}$, which in low-dimensional space is nonlinearly separable. We adopted the random mapping method (RMM) to obtain a linear model in high-dimensional space. Firstly, we used the random mapping to generate a mapping function $g(\mathbf{\Omega_1 U_i})$, where $\mathbf{U_i} = [x_i \ y_i]^{\mathrm{T}}$, $g(\cdot)$ is the sine function $g(\cdot) = \sin(\cdot)$ and $\mathbf{\Omega}_1$ is a 1000×2 matrix denoting a linear transformation. We then defined $\mathbf{v_i} \triangleq \mathbf{\Omega_1 U_i}$ and the vector-valued function $\mathbf{g(v)} = [g(\mathbf{v}_1), \cdots, g(\mathbf{v}_M)]^{\mathrm{T}}$. Here, we further defined a matrix $\mathbf{V} = [\mathbf{v}_1, \cdots, \mathbf{v}_N]$ and a matrix-valued function $\mathbf{G(V)} = [\mathbf{g}(\mathbf{v}_1), \cdots, \mathbf{g}(\mathbf{v}_N)]$. As a result, for the input set $\mathbf{X} = \{(x_i, y_i)\}_{i=1}^{N}$, we could obtain the random mapping matrix $\mathbf{S} = \mathbf{G}(\mathbf{\Omega}_1\mathbf{X}) = \mathbf{G(V)}$. Finally, we took $\mathbf{Z} = \{(z_i)\}_{i=1}^{N}$ as the target value and use $\mathbf{S}$ to generate a general form of the high-dimensional linear model

$$z_{RMM} = \mathbf{B}_1 \sin(\mathbf{\Omega}_1\mathbf{U} + \mathbf{b}_1) + a_1, \ \mathbf{U} = [x \ y]^{\mathrm{T}}, \tag{1}$$

where z_{RMM} is the height determined via the high-dimensional linear model, $\mathbf{B}_1$ is a 1×1000 parameter matrix, $\mathbf{b}_1$ is a 1000×1 parameter matrix, and a_1 is the intercept. We calculated the value of z_{RMM} corresponding to all (x, y) in dataset $\mathbf{D}$, creating the dataset $\mathbf{G} = \{(x_i, y_i, z_{RMMi})\}_{i=1}^{N}$.

B. Treatment of Model Error

The height computed via the high-dimensional linear model was lower than the real altitude, which would increase the risk of UAVs colliding with the mountain during actual flight. Accordingly, an error model was established and used as a compensation term to amend the high-dimensional linear model. The steps taken to handle the error were as follows.

First, the height difference Δz between z_{RMM} and the actual terrain height $z_{\mathbf{D}}$ was calculated as $\Delta z = z_{RMM} - z_{\mathbf{D}}$.

Thus, the error dataset $\mathbf{E}_1 = \{(x_i, y_i, \Delta z_i)\}_{i=1}^{N}$ was obtained.

Immediately thereafter, the error model was established using the RMM on dataset $\mathbf{E}_1$ via

$$\Delta z_{RMM} = \mathbf{B}_2 \sin(\mathbf{\Omega}_2\mathbf{U} + \mathbf{b}_2) + a_2, \ \mathbf{U} = [x \ y]^{\mathrm{T}}, \tag{2}$$

where Δz_{RMM} is the error value, $\mathbf{B}_2$ is a 1×1000 parameter matrix, $\mathbf{\Omega}_2$ is a 1000×2 parameter matrix; $\mathbf{b}_2$ is a 1000×1 parameter matrix, and a_2 is the intercept. (2) was applied as the compensation term for (1) to yield the following amended model

$$Z_1 = \mathbf{B}_1 \sin(\mathbf{\Omega}_1\mathbf{U} + \mathbf{b}_1) + a_1 - \mathbf{B}_2 \sin(\mathbf{\Omega}_2\mathbf{U} + \mathbf{b}_2) - a_2. \tag{3}$$

Using this amended model, the actual height value was subtracted from the value of amended model height to obtain the amended error dataset as $\mathbf{E}_2 = \{(x_i, y_i, \Delta Z_i)\}_{i=1}^{N}$.

Finally, to ensure that the model height value was larger than the actual terrain height, an error value less than 0 was compensated for by a smaller positive constant C.

The ultimate terrain lightweight model was expressed as

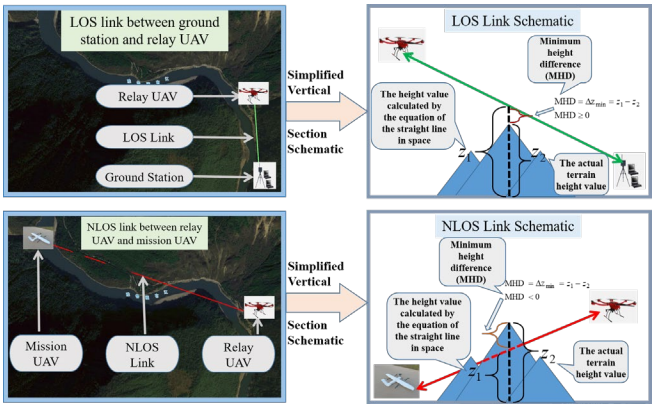

Fig. 3. Concepts and definitions of LOS and NLOS considered in this study.

$$Z = \mathrm{F}(x, y) = \begin{cases} \mathbf{B}_1 \sin(\mathbf{\Omega}_1\mathbf{U} + \mathbf{b}_1) + a_1 - \mathbf{B}_2 \sin(\mathbf{\Omega}_2\mathbf{U} + \mathbf{b}_2) - a_2, \Delta z \geq 0 \\ \mathbf{B}_1 \sin(\mathbf{\Omega}_1\mathbf{U} + \mathbf{b}_1) + a_1 - \mathbf{B}_2 \sin(\mathbf{\Omega}_2\mathbf{U} + \mathbf{b}_2) - a_2 + C, \Delta z \leq 0 \end{cases}. \tag{4}$$

IV. LOS Judgment Model

A. LOS Link and NLOS Link

In this section, to more conveniently and rapidly determine the signal propagation mode between communication nodes in an over-the-horizon observation mission, we construct an LOS judgment model (LJM) based on the LOS links. In a mountainous environment, an LOS link indicates that the connection between communication nodes is not obstructed by the mountain, and an NLOS link indicates that the mountain is interfering with the connection between communication nodes. The existence of an LOS link can be intuitively detected using the LJM, which was defined as the minimum height difference (MHD) between the line connecting the spatial positions of the communication nodes and the actual terrain. Additionally, an LOS link was defined as one in which the MHD was greater than or equal to zero; otherwise, it was an NLOS link. These concepts and definitions are illustrated in Fig. 3.

B. Establishment of the LOS Judgment Model

For calculating the MHD between the relay UAV and the GS, we first constructed the straight line equation as

$$\begin{cases} x = x_g + t_0 \times (x_r - x_g) \\ y = y_g + t_0 \times (y_r - y_g) \\ z = z_g + t_0 \times (z_r - z_g) \end{cases}, \tag{5}$$

where (x_g, y_g, z_g) is the position of the GS (the initial point), (x_r, y_r, z_r) is the position of the relay UAV (the final point), and t_0 is proportionality constant.

Then, n ($n = \mathrm{INT}((x_r - x_g)/d_s)$) points were marked at d_s, where the function $\mathrm{INT}(\cdot)$ indicates that the number is rounded down to the nearest integer.

Next, assume that (x_i, y_i, z_i) is any point among n points, here $i \in 1, 2, \ldots, n$. Calculate parameter $t_i = (x_i - x_g)/(x_r - x_g)$. Compute the height value $z_i = z_g + t_i \times (z_r - z_g)$ corresponding to the i-th point on the spatial connection between the GS and relay UAV. Calculate ΔZ_i of the i-th point as

$$\Delta Z_i = z_i - \mathrm{F}(x_i, y_i), \tag{6}$$

where $\mathrm{F}(x_i, y_i)$ describes the surface elevation value corresponding to the coordinate (x_i, y_i) in the actual elevation map.

Finally, calculate the height differences of the aforementioned n points, and the minimum value of n height differences is the MHD, which was expressed as

$$\mathrm{MHD} = \min\left\{\Delta Z_i\right\}_{i=1}^{n}. \tag{7}$$

V. Minimum Turning Radius Constraints

A. Turning Radius Analysis

Consider the waypoint path defined by the three waypoints $\mathbf{w}_{i-1}, \mathbf{w}_i$ and $\mathbf{w}_{i+1}$. The unit vectors of the waypoint segments $\overline{\mathbf{w}_{i-1}\mathbf{w}_i}$, $\overline{\mathbf{w}_i\mathbf{w}_{i+1}}$ are respectively denoted as

$$\mathbf{q}_i = \frac{\mathbf{w}_{i-1}-\mathbf{w}_i}{\left\|\mathbf{w}_{i-1}-\mathbf{w}_i\right\|}, \mathbf{q}_{i+1} = \frac{\mathbf{w}_{i+1}-\mathbf{w}_i}{\left\|\mathbf{w}_{i+1}-\mathbf{w}_i\right\|}, \tag{8}$$

where $\|\cdot\|$ denotes the Euclidean norm. As shown in Fig. 4, let $\mathcal{C}$ be a circle with a minimum turning radius R. Its center point $\mathbf{w}_C$ lies on the bisector of the angle formed by $\mathbf{w}_{i-1}, \mathbf{w}_i$, and $\mathbf{w}_{i+1}$, such that the circle $\mathcal{C}$ is inscribed with the path segment $\overline{\mathbf{w}_{i-1}\mathbf{w}_i}$ and the path segment $\overline{\mathbf{w}_i\mathbf{w}_{i+1}}$.

The tangent point on $\overline{\mathbf{w}_{i-1}\mathbf{w}_i}$ is donated as $\mathbf{w}_e$, and the tangent point on $\overline{\mathbf{w}_i\mathbf{w}_{i+1}}$ is donated as $\mathbf{w}_s$. Let β denote the angle formed by the three waypoints, and get $\beta = \cos^{-1}(\mathbf{q}_i\mathbf{q}_{i+1}^{\mathrm{T}})$.

To calculate the position of the center point $\mathbf{w}_C$, we first denote the unit vector $\overline{\mathbf{q}}$ of the angle bisector as

$$\overline{\mathbf{q}} = (\mathbf{q}_{i+1}+\mathbf{q}_i)/(\|\,\mathbf{q}_{i+1}+\mathbf{q}_i\,\|). \tag{9}$$

The distance between $\mathbf{w}_i$ and $\mathbf{w}_C$ is: $\left\|\mathbf{w}_C-\mathbf{w}_i\right\| = R/\sin(\beta/2)$, then $\mathbf{w}_C = \mathbf{w}_i + (R/\sin(\beta/2))\overline{\mathbf{q}}$. For $\mathbf{w}_e$, we first calculate the distance between $\mathbf{w}_i$ and $\mathbf{w}_e$ as $\left\|\mathbf{w}_e-\mathbf{w}_i\right\| = R/\tan(\beta/2)$. Then $\mathbf{w}_e$ is given by $\mathbf{w}_e = \mathbf{w}_i + (R/\tan(\beta/2))\mathbf{q}_i$. Therefore, in the same way $\mathbf{w}_s = \mathbf{w}_i + (R/\tan(\beta/2))\mathbf{q}_{i+1}$.

Finally, the trajectory of the fixed-wing UAV consists of the line segment $\overline{\mathbf{w}_{i-1}\mathbf{w}_e}$, arc segment $\overset{\frown}{\mathbf{w}_e\mathbf{w}_s}$, and line segment $\overline{\mathbf{w}_i\mathbf{w}_{i+1}}$, which is represented by the green curve in Fig. 4.

B. Construction of Minimum Turning Radius Constraints

As shown in Fig. 5, there are three situations (a), (b), and (c) in which the circle has no tangent point with the line segments. We define $d(\mathbf{x},\mathbf{y}) = \left\|\mathbf{x}-\mathbf{y}\right\|$ as the distance between $\mathbf{x}, \mathbf{y}$.

In (a), $d(\mathbf{w}_{i-1},\mathbf{w}_i) < d(\mathbf{w}_e,\mathbf{w}_i)$, $d(\mathbf{w}_{i+1},\mathbf{w}_i) > d(\mathbf{w}_s,\mathbf{w}_i)$, and there is no tangent point on the line segment $\overline{\mathbf{w}_{i-1}\mathbf{w}_i}$;

In (b), $d(\mathbf{w}_{i-1},\mathbf{w}_i) > d(\mathbf{w}_e,\mathbf{w}_i)$, $d(\mathbf{w}_{i+1},\mathbf{w}_i) < d(\mathbf{w}_s,\mathbf{w}_i)$, and there is no tangent point on the line segment $\overline{\mathbf{w}_i\mathbf{w}_{i+1}}$;

In (c), $d(\mathbf{w}_{i-1},\mathbf{w}_i) < d(\mathbf{w}_e,\mathbf{w}_i)$, $d(\mathbf{w}_{i+1},\mathbf{w}_i) < d(\mathbf{w}_s,\mathbf{w}_i)$, there is no tangent points both on the $\overline{\mathbf{w}_{i-1}\mathbf{w}_i}$ and $\overline{\mathbf{w}_i\mathbf{w}_{i+1}}$.

Therefore, owing to the minimum turning radius, waypoints $\mathbf{w}_e$ and $\mathbf{w}_s$ must comply with the constraints given by

$$d(\mathbf{w}_{i-1},\mathbf{w}_i) \geq d(\mathbf{w}_e,\mathbf{w}_i), \tag{10}$$

$$d(\mathbf{w}_{i+1},\mathbf{w}_i) \geq d(\mathbf{w}_s,\mathbf{w}_i). \tag{11}$$

C. Extreme Situation

When the angle formed by three waypoints $\mathbf{w}_{i-1}, \mathbf{w}_i$, and $\mathbf{w}_{i+1}$ is 180°, circle $\mathcal{C}$ is tangent to $\overline{\mathbf{w}_{i-1}\mathbf{w}_{i+1}}$ such that $\mathbf{w}_e$ and $\mathbf{w}_s$ coincide with the $\mathbf{w}_i$, as shown in Fig. 5(d). In this case, $\beta/2$ is 90°, and $\tan(\beta/2)$ does not exist. Therefore, in this situation, the fixed-wing UAV flew directly from $\mathbf{w}_{i-1}$ to $\mathbf{w}_{i+1}$.

VI. Cooperative Trajectory Planning

To plan the trajectories of the mission UAV and relay UAV collaboratively,

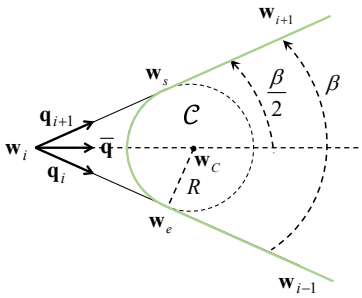

Fig. 4. Inscribed circle between waypoint segments.

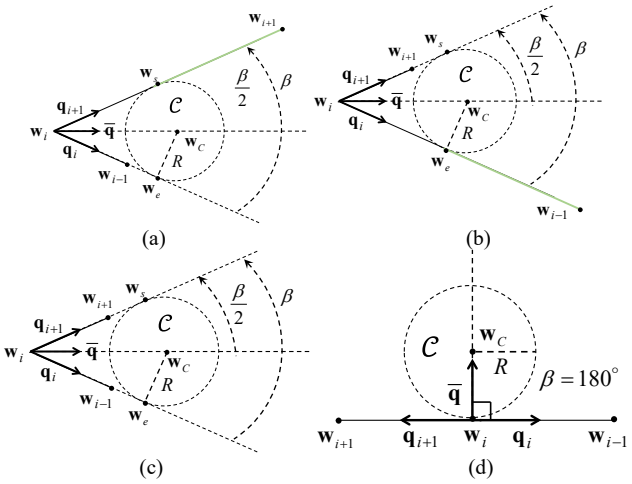

Fig. 5. Situations in (a)(b)(c) the tangent point does not exist; situation in (d) $\beta = 180^\circ$.

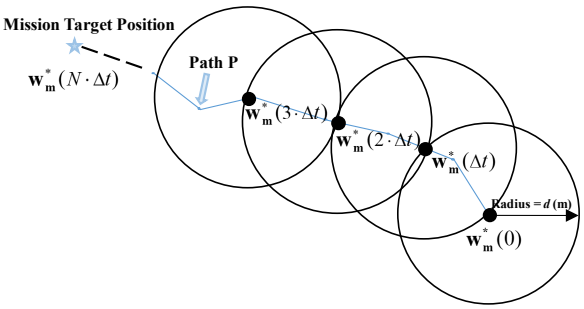

Fig. 6. Schematic of the reference path $\mathbf{P}_m^*$.

the heterogeneous UAVs cooperative communication problem is abstracted into a trajectory planning problem that considers UAV maneuverability, obstacle and collision avoidance, LOS constraints, and minimum turning radius constraints. The total mission time needs to be minimized, because a shorter mission time usually means a lower total system energy consumption. Therefore, we first planned the mission UAV reference path. Then the mission UAV tracked the reference path and constructed an LOS link with the relay UAV by adjusting its position. Finally, A multi-step optimization model was established to plan the trajectories of the mission UAV and relay UAV.

A. Fixed-wing UAV Reference Path Planning

To enable the fixed-wing UAV to arrive at the target position faster, we first used the A-Star algorithm (A*) to plan the shortest path **P** from the starting position to the target position. The grid of A* was a rectangle of 25m×15m in size. During the mission, the fixed-wing UAV flew at a constant speed. To

guarantee the same flight time Δt between any two adjacent waypoints, as shown in Fig. 6, we considered a reference waypoint every d m along path $\mathbf{P}$ from the starting point. Finally, we obtained the reference path as

$$\mathbf{P}_{\mathbf{m}}^{*} = \{\mathbf{w}_{\mathbf{m}}^{*}(0), \mathbf{w}_{\mathbf{m}}^{*}(\Delta t), \ldots, \mathbf{w}_{\mathbf{m}}^{*}(N \cdot \Delta t)\}.$$

B. Multi-step Optimization Model

The multi-step optimization model had a superior predictive performance. When the corner was in front of the UAV, the multi-step optimization model could make decisions in advance so that the UAV maneuvered around the corner smoothly. The mission UAV tracked the reference path and adjusted its position to maintain the LOS link with the relay UAV. Therefore, to obtain better planning results, we built the multi-step optimization model given by

$$\min \sum_{k=1}^{p} \left\| \mathbf{w}_{\mathbf{r}}(t+\Delta t \cdot k) - \mathbf{w}_{\mathbf{r}}(t+\Delta t \cdot (k-1)) \right\| + \omega \times \sum_{k=1}^{p} \left\| \mathbf{w}_{\mathbf{m}}(t+\Delta t \cdot k) - \mathbf{w}_{\mathbf{m}}^{*}(t+\Delta t \cdot k) \right\| \tag{12}$$

$$s.t. \min \left\{ \Delta Z_i(\mathbf{w}_{\mathbf{m}}(t+\Delta t \cdot k), \mathbf{w}_{\mathbf{m}}(t+\Delta t \cdot (k-1))) \right\}_{i=1}^{n} \geq 0 \tag{13}$$

$$\min \left\{ \Delta Z_i(\mathbf{w}_{\mathbf{r}}(t+\Delta t \cdot k), \mathbf{w}_{\mathbf{g}}) \right\}_{i=1}^{n} \geq 0 \tag{14}$$

$$\min \left\{ \Delta Z_i(\mathbf{w}_{\mathbf{r}}(t+\Delta t \cdot k), \mathbf{w}_{\mathbf{m}}(t+\Delta t \cdot k)) \right\}_{i=1}^{n} \geq 0 \tag{15}$$

$$((\Delta \mathbf{w}_{\mathbf{r},k}) \mathbf{A} (\Delta \mathbf{w}_{\mathbf{r},k})^{\mathrm{T}})^{1/2} \leq 1 \tag{16}$$

$$d(\mathbf{w}_{\mathbf{m}}(t+\Delta t \cdot (k-2)), \mathbf{w}_{\mathbf{m}}(t+\Delta t \cdot (k-1))) \geq d(\mathbf{w}_{e}(t+\Delta t \cdot (k-1)), \mathbf{w}_{\mathbf{m}}(t+\Delta t \cdot (k-1))) \tag{17}$$

$$d(\mathbf{w}_{\mathbf{m}}(t+\Delta t \cdot k), \mathbf{w}_{\mathbf{m}}(t+\Delta t \cdot (k-1))) \geq d(\mathbf{w}_{s}(t+\Delta t \cdot (k-1)), \mathbf{w}_{\mathbf{m}}(t+\Delta t \cdot (k-1))) \tag{18}$$

where $\mathbf{w}_{\mathbf{r}}, \mathbf{w}_{\mathbf{m}}, \mathbf{w}_{\mathbf{g}}, \mathbf{w}_{\mathbf{m}}^{*}$ represent the waypoint of the relay UAV, the waypoint of the mission UAV, the position of GS, and the reference waypoint of the mission UAV, respectively; $\Delta \mathbf{w}_{\mathbf{r},k} = \mathbf{w}_{\mathbf{r}}(t+\Delta t \cdot k) - \mathbf{w}_{\mathbf{r}}(t+\Delta t \cdot (k-1))$ and $\mathbf{A} = diag(a^{-2}\ b^{-2}\ c^{-2})$ is a diagonal matrix, a, b, c are the maximum flight distance in X, Y, Z directions, respectively; $\mathbf{w}_{\mathbf{e}}, \mathbf{w}_{\mathbf{s}}$ are tangent points; $t = 0, \Delta t, 2 \cdot \Delta t, \ldots, N \cdot \Delta t$. Equation (12) is the objective function, where p is the predictive step; ω represents the penalty factor for the mission UAV deviating from the optimal trajectory; ω is used to balance the relay UAV flight distance and the deviation of the mission UAV from the reference path. Equations (13) ~ (18) represent the constraints of this problem. The first is the collision avoidance constraint, which was used to prevent the mission UAV from crashing into the mountains. The second and third constraints ensure the relay UAV to constructing LOS links between the GS and mission UAV. The fourth constraint considers the maximum flight velocity of the relay UAV. The last two equations represent the minimum turning radius constraints required for the fixed-wing UAV. Finally, the relay and mission UAV trajectories were planned using the particle swarm optimization algorithm.

VII. Experimental Results

Before conducting the experiment, we established the following experimental conditions:

1) For the fixed-wing UAV, the flight altitude was 50 m, the flight velocity was 20 m/s, and the minimum turning radius was 20 m. For the multirotor UAV, the maximum horizontal velocity was 10 m/s and the maximum vertical velocity was 5 m/s.
2) The time interval Δt was 5 s, which is suitable for this large-scale application scenario.
3) All experiments were conducted on a laptop with an Intel i7 CPU and 16GB of RAM.

A. Terrain Lightweight Modeling

a). Error Processing

Experiments were performed to build a terrain model and verify the effectiveness of the error treatment. First, the terrain modeling in dataset **D** of the actual task area and the data volume were reduced from 842236 sets of coordinate points to 4001 parameter data. Hence, the data storage volume decreased by a factor of approximately 210. Through a comparison of the 3D point cloud map of the real mission area (Fig. 7(a)) with the high-dimensional linear model (Fig. 7(b)), the height value calculated by the high-dimensional linear model was found to be smaller than the actual elevation value, thus it was important to perform an error treatment. The error distribution is illustrated in Fig. 7(c).

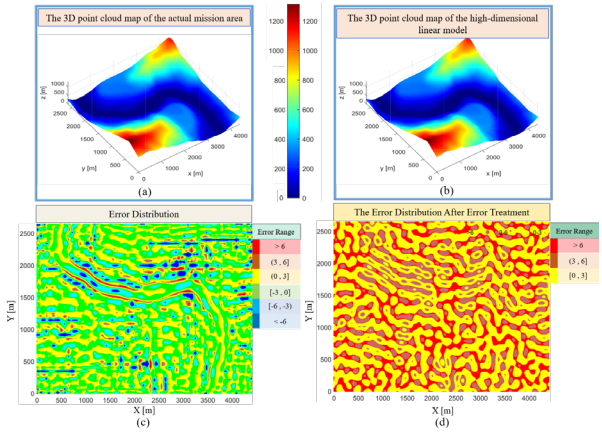

Fig. 7. (a) is 3D point cloud map of the actual mission area, (b) is 3D point cloud map of the high-dimensional linear model; and (c) is the error distribution, (d) is the error distribution after error treatment.

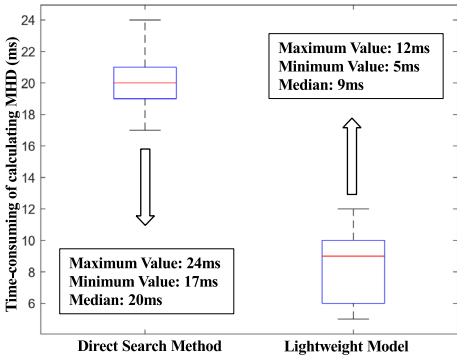

Fig. 8. Time consumption of the DSM and LM.

TABLE I
THE ERROR SITUATION OF THE HIGH-DIMENSIONAL LINEAR MODEL AND THE MODIFIED MODEL

	High-dimensional Linear Model	Modified Model
Maximum Error(m)	23.1	6.2
Minimum Error(m)	-25.9	-7.8
Average Error(m)	2.1707	1.355

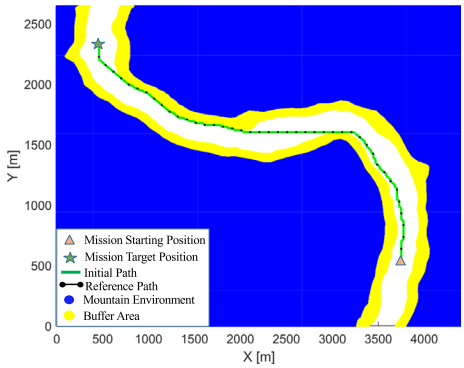

Fig. 9. Schematic of the reference path.

From Table I, the margin of error was reduced from [-25.9, 23.1] to [-7.8, 6.2], and the error distribution became more uniform. For error values less than 0 plus 7.8 meters, the ultimate error distribution after error treatment is shown in Fig. 7(d). The figure indicates that the error values were all greater than 0. Hence, the height values computed from the terrain lightweight model were all greater than the actual elevation values, which prevented the relay UAV from colliding with the mountains while flying along the relay trajectory.

b). Advantages of Lightweight Model

The lightweight model (LM) has the advantages of a short computational time and high efficiency. Because any point $N_i(x_i, y_i, z_i)$ on the line connecting the relay UAV and the GS is not necessarily a point in dataset **D**, the direct search method (DSM) selects the maximum z-value point within a 5m × 5m area as N_i in the XOY plane, with (x_i, y_i) as the center. However, the LM brings (x_i, y_i) in the high dimensional linear function directly to calculate the elevation value z_{RMMi}, and uses (x_i, y_i, z_{RMMi}) as N_i. According to the construction of the LJM, the minimum height difference (MHD) between 45 groups of relay UAV trajectory points and mission UAV trajectory points were calculated by the DSM and LM, respectively, and the time consumed in each cycle was recorded. Fig. 8 shows the comparison of the time spent on calculating the MHD by the two methods. The total time required by the DSM to compute the mission was 900 ms, while that of the LM was 405 ms. Hence, the computation time of the LM was lower than that of the DSM by 55%.

B. The Reference Path Planning for The Mission UAV

In this study, the mission path was planned using the A-star algorithm. To prevent the mission UAV from crashing into mountains due to small deviations in map data or external disturbances such as strong winds, we added the buffer area and planned a new mission path, which is the green path in Fig. 9. According to the given experimental conditions, the velocity of the mission UAV was 20 m/s, the time interval Δt was 5 s, thus the distance d between any two adjacent waypoints is 100 m. Finally, the reference path $\mathbf{P}_\mathbf{m}^*$ consisted of 45 waypoints, which are shown as the black path in Fig. 9.

C. Multi-step Optimization Model for Heterogeneous UAVs

For the multi-step optimization model, the weight factor ω and predictive step p were the two key factors affecting the results. In this section, we discuss the impact of the changes in ω and p on the experimental results, and select the appropriate values for ω and p according to the actual simulation results in order to optimize the results.

a). Appropriate Weight Factor ω

The weight factor ω has a significant effect on the trajectory planning of the relay UAV and mission UAV. There were 45 reference waypoints in total. During the simulation, if the mission UAV did not arrive at the mission target position within 225 s, we used the mission target point as the reference waypoint until the mission UAV arrived at the mission target position. For the following experiment, let the predictive step p=1.

Fig. 10(a) indicates that ω has an effect on both the total mission time (blue curve) and the total flight distance of the relay UAV (orange curve). As ω increased, the total mission time decreased and reached the shortest mission time when ω increased to a certain value, the shortest time was 225 s; the overall trend was that the total flight distance of the relay UAV increased. When ω was small, more attention was given to the relay UAV to decrease the flight distance. At this stage, the mission UAV deviated from the reference path to maintain LOS communication with the relay UAV, but it deviated too much to arrive at the mission target position within 45 computing cycles. Thus, the total mission time was more than 225 s. When ω was large, more attention was given to the deviation of the mission UAV; the mission UAV effectively tracked the reference path and arrived at the mission target position within 45 computing cycles, and the relay UAV increased the flight distance to maintain LOS link with the mission UAV.

Fig. 10(b) shows that, when ω was small, the mission UAV poorly tracked the reference path and deviated from the reference path significantly, but it tracked the reference path well when ω was large. Thus, as ω increased, the mission UAV more effectively tracked the reference path, thereby reducing mission time. According to Fig. 10(c), when ω was small, the relay UAV had a shorter trajectory, which reduced the relay UAV endurance pressure. When ω was large, the relay UAV had a longer trajectory, resulting in increased energy consumption. Therefore, an increase in ω lead to an increase in the flight distance of the relay UAV.

To reduce total mission time and the relay UAV endurance pressure, an appropriate ω is to be determined. When $\omega = 2.1$, the total mission time was 225 s, the total flight distance was 971 m, representing the minimum flight distance. Therefore, $\omega = 2.1$ was an appropriate value in this mission scenario, and the following experimental results were obtained with $\omega = 2.1$.

b). Appropriate Predictive Step p

Theoretically, more predictive steps will lead to better results, while the variables of the algorithm will increase exponentially, and the running time of the algorithm will increase significantly as well.

Fig. 11 shows that as p increased, the total flight distance of the relay UAV decreased, and the run time of the algorithm increased. According to (12), the number of variables was proportional to p. The search range of the particle swarm and the number of iterations in each cycle of the algorithm also increased.

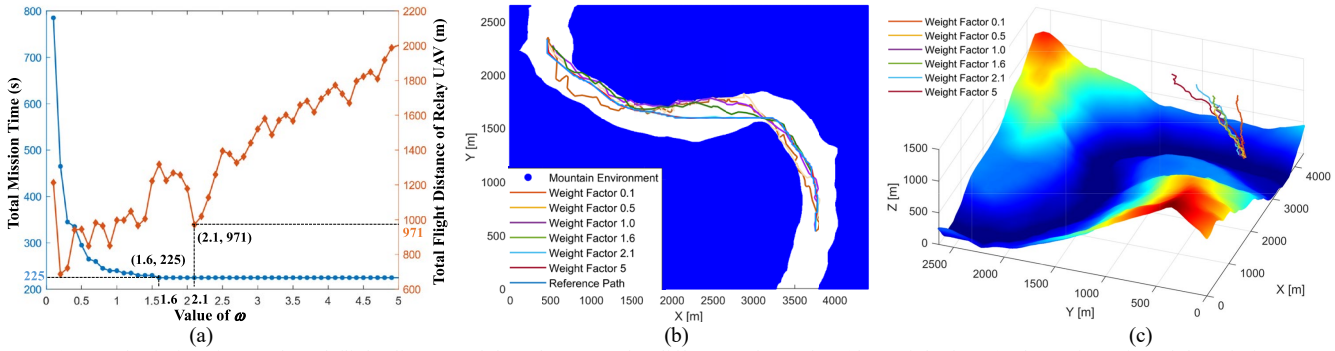

Fig. 10. (a) Total mission time and total flight distance of the relay UAV for different values of ω (the weight factor). (b) Trajectories of the mission UAV for different values of ω. (c) Trajectories of the relay UAV for different values of ω.

TABLE II

THE COMPARISON OF RUN TIME OF ALGORITHM AND TOTAL FLIGHT DISTANCE

	Increased Run Time (%)	Decreased Flight Distance (%)
p =2	907.79	11.84
p =3	2368.38	21.63
p =4	5779.35	22.25
p =5	15015.79	23.48

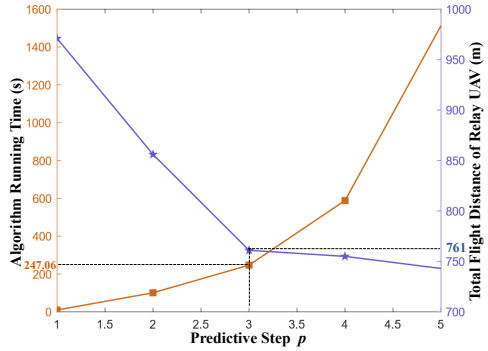

Fig. 11. Algorithm running time and total flight distance of the relay UAV for different values of p.

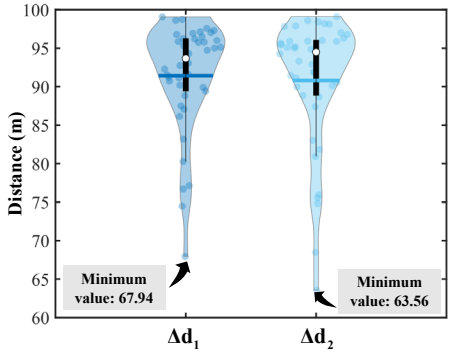

Fig. 12. Difference results for $\Delta \mathbf{d_1}$, $\Delta \mathbf{d_2}$.

TABLE III

PERFORMANCE COMPARISON OF BASIC METHOD AND COOPERATIVE PLANNING STRATEGY

	Total Mission Time (s)	Total Flight Distance (m)
BM	450	1322
CPS	225	761

At the same time, all the constraints in (13) ~ (18) needed to be satisfied. All of the above were key factors that lead to the increase of the run time of the algorithm.

For the range $1 \le p \le 3$, the total flight distance decreased significantly and the run time of the algorithm rose steadily. In contrast, for the range $3 < p \le 5$, the total flight distanced slightly, but the run time of the algorithm significantly increased. The results compared to $p = 1$ are shown in Table II, as p increased, the run time of the algorithm continued to significantly increase; the total flight distance changed from a significant decrease to a slow decrease.

Considering both the computational cost and the actual predictive step requirements, if the predictive step was too small, the effect was poor; if the predictive step was too long, it wasted computing resources. Therefore, $p = 3$ was an appropriate predictive step in this mission scenario.

c). Performance Comparison Between Basic Method and Cooperative Planning Strategy

In previous studies, we used the basic method (BM) for experiments which only planned the trajectory of the relay UAV, leading to unsatisfactory experimental results. Therefore, we proposed cooperative planning strategy (CPS) which planned the trajectories of the mission UAV and relay UAV cooperatively to maintain LOS communication between the mission UAV and GS. We compare the BM and CPS in terms of the total mission time and the total flight distance of the relay UAV. From Table III, the total mission time of the CPS has been reduced by 50%, and the total flight distance of the relay UAV has been reduced by 42.44%. Therefore, the proposed CPS can effectively reduce the total mission time and endurance pressure of relay UAV.

d). Minimum Turning Radius Constraints of Fixed-wing UAV

To verify the effectiveness of the minimum turning radius constraints, we first let $\Delta \mathbf{d_1} = d(\mathbf{w}_{i-1}, \mathbf{w}_i) - d(\mathbf{w}_e, \mathbf{w}_i)$, and $\Delta \mathbf{d_2} = d(\mathbf{w}_{i+1}, \mathbf{w}_i) - d(\mathbf{w}_s, \mathbf{w}_i)$, calculated $\Delta \mathbf{d_1}$, $\Delta \mathbf{d_2}$ for each group, and compared their relationship to 0. In Fig. 12, the minimum value of $\Delta \mathbf{d_1}$ is 67.94 m and the minimum value of $\Delta \mathbf{d_2}$ is 63.56 m, both of which were far greater than 0. Therefore, the trajectory planning was reasonable and always satisfied inequality constraints. In addition, the planned trajectory was flyable for the fixed-wing UAV.

VIII. CONCLUSION AND FUTURE WORK

In this study, a cooperative planning method was proposed to maintain the LOS communication between heterogeneous multi-UAVs in complex mountainous environments with limited communication. First, the terrain lightweight model was able to reduce the data storage requirements. The problem of the height value of the lightweight model being lower than the

actual altitude was solved by establishing an error treatment model. Then, the combination of the proposed LOS judgment model and the terrain lightweight model ensured that the communication links were LOS links. Next, the minimum turning radius constraints were constructed to obtain the flyable trajectory for the fixed-wing UAV. The multi-step optimization model of UAV autonomous trajectory planning was designed to solve the problem of communication link interruptions in complex mountainous environments. Finally, simulations were conducted to confirm the effectiveness of the proposed cooperative planning method for heterogeneous UAVs.

In future work, we will adopt a distributed modeling strategy to improve modeling accuracy: a large modeling area is divided into several small areas, and the high-dimensional linear model is established for each small area. We will combine the sequence quadratic program and particle swarm optimization algorithms to reduce the run time of the algorithm for the multi-objective optimization model, considering both the algorithm accuracy and real-time performance. The cooperative operation of multi-relay and multi-mission UAVs will also be considered. Finally, we will consider more complex missions, in which the mission UAV is required to replan and adjust the mission while in flight.

REFERENCES

[1] J. Qin, Q. Ma, Y. Shi and L. Wang, "Recent Advances in Consensus of Multi-Agent Systems: A Brief Survey," *IEEE Trans. Ind. Electron.*, vol. 64, no. 6, pp. 4972-4983, June 2017.

[2] P. Shi and B. Yan, "A Survey on Intelligent Control for Multiagent Systems," *IEEE Trans. Ind. Electron.*, vol. 51, no. 1, pp. 161-175, Jan. 2021.

[3] G. E. G. Padilla, K. J. Kim, S. H. Park and K. H. Yu, "Flight Path Planning of Solar-Powered UAV for Sustainable Communication Relay," *IEEE Rob. Autom. Lett.*, vol. 5, no. 4, pp. 6772-6779, Oct. 2020.

[4] X. Chen et al., "UAV Relayed Covert Wireless Networks: Expand Hiding Range via Drones," *IEEE Network*, vol. 36, no. 4, pp. 226-232, July 2022.

[5] F. Cheng, G. Gui, N. Zhao, Y. Chen, J. Tang and H. Sari, "UAV-Relaying-Assisted Secure Transmission With Caching," *IEEE Trans. Commun.*, vol. 67, no. 5, pp. 3140-3153, May 2019.

[6] F. Cheng, G. Gui, N. Zhao, Y. Chen, J. Tang and H. Sari, "UAV-Relaying-Assisted Secure Transmission With Caching," *IEEE Trans. Commun.*, vol. 67, no. 5, pp. 3140-3153, May 2019.

[7] Elijah, Thato, et al, "A review on control and maneuvering of cooperative fixed-wing drones," *Int. J. Dyn. Control.*, vol. 9, pp. 1332-1349, 2021.

[8] R. Rashad, J. Goerres, R. Aarts, J. B. C. Engelen and S. Stramigioli, "Fully Actuated Multirotor UAVs: A Literature Review," *IEEE Rob. Autom. Mag.*, vol. 27, no. 3, pp. 97-107, Sept. 2020.

[9] N.H. Ranchagoda, K. Sithamparanathan, M. Ding, A. Al-Hourani and K.M. Gomez, "Elevation-angle based two-ray path loss model for Air-to-Ground wireless channels," *Veh. Commun.*, vol. 32, 2021.

[10] X. Cai, "An Empirical Air-to-Ground Channel Model Based on Passive Measurements in LTE," *IEEE Trans. Veh. Technol.*, vol. 68, no. 2, pp. 1140-1154, Feb. 2019.

[11] Q. Zhu, "Geometry-Based Stochastic Line-of-Sight Probability Model for A2G Channels Under Urban Scenarios," *IEEE Trans. Antennas Propag.*, vol. 70, no. 7, pp. 5784-5794, July 2022.

[12] A. Al-Hourani, S. Kandeepan, and S. Lardner, "Optimal LAP altitude for maximum coverage," *IEEE Wireless Commun. Lett.*, vol. 3, no. 6, pp. 569-572, Dec. 2014.

[13] L. Zhu, J. Zhang, Z. Xiao, et al. "Millimeter-Wave Full-Duplex UAV Relay: Joint Positioning, Beamforming, and Power Control," *IEEE J. Sel. Areas Commun.*, vol. 38, no. 9, pp. 2057-2073, 2020.

[14] M. Joel, Esposito and W. D. Thomas, "Maintaining wireless connectivity constraints for swarms in the presence of obstacles," in *Proc. Int. Conf. Robot. Automat.*, pp.946-951, 2006.

[15] P. Ladosz, H. Oh, G. Zheng and W. Chen, "A Hybrid Approach of Learning and Model-Based Channel Prediction for Communication Relay UAVs in Dynamic Urban Environments," *IEEE Rob. Autom. Lett.*, vol. 4, no. 3, pp. 2370-2377, July 2019.

[16] Y. Ning and R. Chen, "Secure UAV Relay Communication via Power Allocation and Trajectory Planning," *IEEE Syst. J.*, pp. 1-10, 2022.

[17] Q. Luo, T. H. Luan, W. Shi and P. Fan, "Deep Reinforcement Learning Based Computation Offloading and Trajectory Planning for Multi-UAV Cooperative Target Search," *IEEE J. Sel. Areas Commun.*, vol. 41, no. 2, pp. 504-520, Feb. 2023.

[18] Huang, Liwei, et al, "A novel coordinated path planning method using k-degree smoothing for multi-UAVs," *Appl. Soft Comput.*, vol. 48, pp. 182-192, 2016.

[19] E. Besada-Portas, L. de la Torre, J. M. de la Cruz and B. de Andrés-Toro, "Evolutionary Trajectory Planner for Multiple UAVs in Realistic Scenarios," *IEEE Trans. Rob.*, vol. 26, no. 4, pp. 619-634, Aug. 2010.

[20] Elijah, Thato, et al. "A review on control and maneuvering of cooperative fixed-wing drones," *Int. J. Dyn. Control*, vol. 9, pp. 1332-1349, 2021.

[21] X. Liu, "A Unified Framework for Large-scale Occupancy Mapping and Terrain Modeling using RMM," *IEEE Rob. Autom. Lett.*, vol. 7, no. 2, pp. 5143-5150, 2022.

[22] T. Ding, M. Ding, G. Mao, Z. Lin, D. López-Pérez and A. Y. Zomaya, "Uplink Performance Analysis of Dense Cellular Networks With LoS and NLoS Transmissions," *IEEE Trans. Wireless Commun.*, vol. 16, no. 4, pp. 2601-2613, April 2017.

[23] H. Tataria, P. J. Smith, L. J. Greenstein, P. A. Dmochowski and M. Matthaiou, "Impact of Line-of-Sight and Unequal Spatial Correlation on Uplink MU-MIMO Systems," *IEEE Wireless Commun. Lett.*, vol. 6, no. 5, pp. 634-637, Oct. 2017.

[24] E. P. Anderson, R. W. Beard and T. W. McLain, "Real-time dynamic trajectory smoothing for unmanned air vehicles," *IEEE Trans. Control Syst. Technol.*, vol. 13, no. 3, pp. 471-477, May 2005.

[25] Fransen, Karlijn, and J. V. Eekelen, "Efficient path planning for automated guided vehicles using A*(Astar) algorithm incorporating turning costs in search heuristic," *Int. J. Prod. Res.*, 2021, pp. 1-19.

[26] Wang, Feng, Heng Zhang, and Aimin Zhou. "A particle swarm optimization algorithm for mixed-variable optimization problems," *Swarm Evol. Comput.*, vol. 60, 2021, Art. no. 100808.

[27] Jenny, Bernhard, S. Bojan and T. Patterson, "A compromise aspect-adaptive cylindrical projection for world maps," *Int. J. Geogr. Inf. Sci.*, vol. 29, no. 6, pp. 935-952, 2015.